Three-body Faddeev calculations for ${}^{6}_{\Lambda\Lambda}$He and ${}^{6}_{\Omega\Omega}$He hypernuclei

Faisal Etminan[1] M. R. Hadizadeh[2]

[1] Department of Physics, Faculty of Sciences, University of Birjand, Birjand 97175-615, Iran
[2] College of Engineering, Science, Technology and Agriculture, Central State University, Wilberforce, OH, 45384, USA
Department of Physics and Astronomy, Ohio University, Athens, OH, 45701, USA

Abstract: We study the ground-state properties of ${}^{6}_{YY}$He double hyperon for ${}^{6}_{\Lambda\Lambda}$He and ${}^{6}_{\Omega\Omega}$He nuclei in a three-body model ($Y+Y+\alpha$). We solve two coupled Faddeev equations corresponding to three-body configurations $(\alpha Y, Y)$ and (YY, α) in configuration space with the hyperspherical harmonics expansion method by employing the most recent hyperon-hyperon interactions obtained from lattice QCD simulations. Our numerical analysis for ${}^{6}_{\Lambda\Lambda}$He, using three $\Lambda\Lambda$ lattice interaction models, leads to a ground state binding energy in the domain $(-7.468, -7.804)$ MeV and the separations $\langle r_{\Lambda-\Lambda}\rangle$ and $\langle r_{\alpha-\Lambda}\rangle$ in the domains $(3.555, 3.629)$ fm and $(2.867, 2.902)$ fm, correspondingly. The binding energy of double-Ω hypernucleus ${}^{6}_{\Omega\Omega}$He leads to -67.21 MeV and consequently to smaller separations $\langle r_{\Omega-\Omega}\rangle = 1.521$ fm and $\langle r_{\alpha-\Omega}\rangle = 1.293$ fm. Besides the geometrical properties, we study the structure of ground-state wave functions and show that the main contributions are from the $s-$wave channels. Our results are consistent with the existing theoretical and experimental data.

Keywords: $\Omega\Omega(^1S_0)$ potential, multi-strangeness nucleus, cluster model, hyperspherical harmonics

PACS: 1 – 3 PACS codes (Physics and Astronomy Classification Scheme, https://publishing.aip.org/publishing/pacs/pacs-2010-regular-edition/)

1 Introduction

While hyperons, baryons with a strangeness content, play an important role in compact star mergers and core-collapse events [1], there are limited experimental data on doubly strange hypernuclear systems, and the systems containing higher strangeness are almost unknown. While different phenomenological models have been developed for the nucleon-hyperon (NY) and hyperon-hyperon (YY) interactions, recent developments in computational technologies and theoretical progress in Lattice QCD methods facilitated the derivation of ΩN, $\Omega\Omega$, $\Lambda\Lambda$, and $N\Xi$ interactions [2–4], close to the physical pion masses $m_\pi \simeq 146$ MeV and Kaon masses $m_k \simeq 525$ MeV, by the HAL QCD Collaboration [5, 6] where their physical values are $m_\pi \simeq 135$ MeV and $m_k \simeq 497$ MeV. Of course, the $N\Omega$ and di-Ω interaction were suggested and predicted before the lattice QCD simulation in [7, 8].

The potentials are obtained on a large space-time volume $L^4 = (8.1 \text{ fm})^4$ with a lattice spacing $a = 0.0846$ fm. While there are sophisticated calculations to study ${}^{6}_{\Lambda\Lambda}$He hypernucleus [9–18], in this work, we examine the HAL QCD $\Lambda\Lambda$ interactions, which are the most consistent potential with the LHC ALICE data [19, 20], to study the ground state properties of the ${}^{6}_{\Lambda\Lambda}$He hypernucleus. Similarly, we explore the $\Omega\Omega\alpha$ system with lattice QCD-based interactions.

Because of following motivation we become curious to explore possible implications of the attractive nature of the ΩN and $\Omega\Omega$ interactions on few-body $\Omega\Omega\alpha$ systems on the basis of first-principle lattice QCD-based interactions. In few-body systems the presence of additional nucleons may increase the binding. There are straightforward examples in nature. Although there are no dibaryon bound states with strangeness $= -1$ (Λ-nucleon system), hypertriton ${}^{3}_{\Lambda}$H, consisting of a neutron, a proton, and a Λ-particle, is bound with a separation energy of 0.41 ± 0.12 MeV [21, 22]. In the case of strangeness $= -2$, in systems containing Ξ-particles, an enhancement in the binding energy per baryon is observed by increasing the number of nucleons [23–25]. The Extended-Soft-Core (ESC08c) model of Nijmegen interaction [26] supports the bound states of ΞN and ΞNN ($T = 1/2$, $J^\pi = 3/2^+$) with energies -1.56 and -17.2 MeV, respectively [23, 24, 27]. Recently Garcilazo *et al.* have implemented ΩN and $\Omega\Omega$ interactions derived by the HAL QCD Collaboration [2, 3, 28] to study three-body systems containing more strangeness number, *i.e.* ΩNN and $\Omega\Omega N$ with strangeness $= -3$ and -6 [26]. As a result, they obtained Ωd $(0,\ 5/2^+)$ bind-

Received 31 June 2015

1) E-mail: fetminan@birjand.ac.ir
2) E-mail: mhadizadeh@centralstate.edu

ing energy of about -20 MeV and two resonance states Ωnn $(1,\ 3/2^+)$ and $\Omega\Omega N$ $(1/2,\ 1/2^+)$, with resonance energies of 1 and 4.6 MeV, correspondingly. Besides the Ω-deuteron bound state, $\Omega\Omega\alpha$ bound state would be an interesting system to benchmark the $\Omega\alpha$ and $\Omega\Omega$ interactions in a three-body system.

As the femtoscopic analysis of two-particle correlation functions in heavy-ion collisions provides information on hadron-hadron interactions at low energies[29, 30], investigating the ${}^{6}_{\Omega\Omega}$He system can also be interesting for this purpose. The correlation function in multi-strange systems such as $\Lambda\Lambda$ [31, 32] and $p\Omega$ [20, 33, 34] have been measured recently in high-energy nuclear collisions, and as the next step in the femtoscopic analyses, the hadron-deuteron correlation functions would be promising. Actually, experimental investigations of correlations for pd, dd and even for light nuclei have been already performed [35–37], and for K^-d is in advance [38, 39], and Λd correlation function is on the agenda [40, 41]. A method to probe the momentum correlation functions of $\Omega\Omega$ is proposed in Ref. [42]. And very recently, the production of ΩNN and $\Omega\Omega N$ in ultra-relativistic heavy-ion collisions using the Lattice QCD ΩN, $\Omega\Omega$ potentials studied in Ref. [43]. Since the di-Omega appears with the binding energy about 1.6 MeV in ${}^1S_0$ channel [2], there is a possibility that our results could help the future study of $\Omega\Omega-\alpha$ (like $d-\alpha$[44]) two-particle momentum correlation functions, and can be measured in high energy heavy-ion collisions. We explore this hypothetical system for the first time, and to the best of our knowledge, there is no other study on this system.

In the present work, we study the ground state properties of ${}^{6}_{\Lambda\Lambda}$He and ${}^{6}_{\Omega\Omega}$He hypernuclei as a three-body $(\alpha+Y+Y)$ bound state. To do so, we solve two coupled Faddeev equations in configuration space with the hyperspherical harmonics expansion method to calculate the ground state binding energy and the geometrical structures of these hypernuclei. In our study, we use the HAL QCD $\Lambda\Lambda$ and $\Omega\Omega$ interactions, Isle-type Gaussian potential is employed for $\alpha\Lambda$ interactions and a Woods-Saxon type potential is used for $\alpha\Omega$ interaction.

In 2001, the KEK emulsion/scintillating-fiber hybrid experiment [45], known as the Nagara event, reported a uniquely identified double-Λ hypernucleus ${}^{6}_{\Lambda\Lambda}$He with binding energy of -7.25 ± 0.19 MeV. The re-analysis of the Nagara event using the new Ξ mass of 1321.71 MeV [46], revised the binding energy to -6.91 ± 0.16 MeV [47, 48], considerably shallower than the earlier measured value -10.9 ± 0.8 MeV [49]. In the recent J-PARC E07 experiment emulsion analysis, several hypernuclear events have been observed. For example, the Be double Λ hypernucleus has been identified as an event called the "MINO event" [50], and a new Ξ-nuclear deeply bound state has been reported [51]. Furthermore, the high precision spectra for light to heavy multi-strange hypernuclei are planned in the future to be measured at JLab and with the new high-intensity high-resolution line at [51, 52].

Hiyama *et al.* performed a three-body calculation for $\Lambda+\Lambda+{}^4$He, with the Gaussian expansion method, using properly tuned $\Lambda\Lambda$ Nijmegen interactions to reproduce the Nagara event data [9, 10]. Nemura *et al.* studied $\Lambda\Lambda$ hypernuclei with the stochastic variational method using effective phenomenological ΛN and $\Lambda\Lambda$ potentials [11, 12]. Moreover, Filikhin *et al.* have studied ${}^{6}_{\Lambda\Lambda}$He by solving the differential Faddeev equations (DFE) in configuration space using different models of Nijmegen YY interactions [13–16]. Recently double-strangeness hypernuclei are studied in an effective field theory approach using the stochastic variational method at leading order [17] and with the Jacobi no-core shell model at the next-to-leading order [18]. The cluster structure of light hypernuclei [53, 54] has been studied with different methods, including the generator coordinate method [55], the orthogonality condition model [56], the Gaussian expansion method [57, 58], and Tohsaki-Horiuchi-Schuck-Röpke wave function approach [59].

The Faddeev-Yakubovsky (FY) equations are extensively used to study the structure of three- and four-body bound states, with identical and non-identical particles, in different sectors of physics [60–65]. FY equations are solved with different techniques, like direct projection in momentum space [66], hyperspherical harmonics (HH) [67], adiabatic hyperspherical [68], and variational methods [69, 70]. The HH method has been implemented to study the complex structure of ^{6}He and ^{11}Li halo nuclei in a three-body picture [67, 71], and in this work, we apply this method to study the ground state properties of double hyperon nuclei in a three-body picture as $Y+Y+\alpha$.

In Sec. 2, we briefly review the HH formalism for $Y+Y+\alpha$ three-body bound state. In Sec. 3, we introduce YY and αY two-body potentials used to study the structure of double-hyperon nuclei. Our numerical results for the ground state binding energies and geometrical properties of ${}^{6}_{\Lambda\Lambda}$He and ${}^{6}_{\Omega\Omega}$He hypernuclei are presented and discussed in Sec. 4. A summary and outlook is provided in Sec. 5.

2 Three-body Faddeev equations in hyperspherical coordinates

The total wave function $\Psi^{j\mu}$ of the three-body system $(YY\alpha)$ for a given total angular momentum j by projection μ, composed of two Y particles and one α particle,

is given as a sum of three Faddeev components $\psi_i^{j\mu}$

$$\Psi^{j\mu} = \sum_{i=1}^{3} \psi_i^{j\mu}(\boldsymbol{x}_i, \boldsymbol{y}_i). \quad (1)$$

Each component $\psi_i^{j\mu}$ is expressed in terms of two Jacobi coordinates $(\boldsymbol{x}_i, \boldsymbol{y}_i)$, and can be obtained from the solution of coupled Faddeev equations

$$(H_0 - E)\psi_i^{j\mu} + V_{jk}\left(\psi_i^{j\mu} + \psi_j^{j\mu} + \psi_k^{j\mu}\right) = 0, \quad (2)$$

where H_0 is the free Hamiltonian, E is 3B binding energy, and V_{jk} is the two body interaction (both the Coulomb and nuclear interactions) between the corresponding pair. The indexes i, j, k run through $(1,2,3)$ in circular order. To solve the coupled Faddeev equations (2) in configuration space, one needs two different sets of Jacobi coordinates $(\mathbf{x}_1, \mathbf{y}_1)$ and $(\mathbf{x}_3, \mathbf{y}_3)$, shown in Fig. 1, defined by

$$\begin{aligned} \mathbf{x}_i &= \sqrt{A_{jk}}\,\mathbf{r}_{jk} = \sqrt{A_{jk}}\,(\mathbf{r}_j - \mathbf{r}_k), \\ \mathbf{y}_i &= \sqrt{A_{(jk)i}}\,\mathbf{r}_{(jk)i} = \sqrt{A_{(jk)i}}\,\left(\mathbf{r}_i - \frac{A_j\mathbf{r}_j + A_k\mathbf{r}_k}{A_j + A_k}\right), \end{aligned} \quad (3)$$

where $\mathbf{r}_i$ is the position vector of particle i, $\mathbf{r}_{jk}$ is the relative distance between the pair particles (jk), and $\mathbf{r}_{(jk)i}$ is the distance between the spectator particle i and the center of mass of pair (jk). The reduced masses are $A_{jk} = \frac{A_j A_k}{A_j + A_k}$ and $A_{(jk)i} = \frac{(A_j + A_k)A_i}{A_i + A_j + A_k}$, where $A_i = \frac{m_i}{m}$, $m = 1$ a.m.u., and m_i is the mass of particle i in a.m.u.

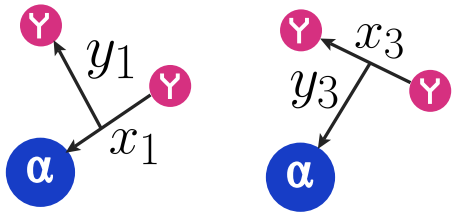

Fig. 1: Two sets of Jacobi coordinates $(Y\alpha, Y)$ and (YY, α) for a description of the $YY\alpha$ three-body system.

The projection of coupled Faddeev equations onto the Jacobi coordinates $(\mathbf{x}_i, \mathbf{y}_i)$ leads to two-dimensional partial differential equations that can be transformed into two sets of coupled one-dimensional equations using the hyperspherical coordinates (ρ_i, Ω_i). The hyperradius is defined by $\rho_i^2 = x_i^2 + y_i^2$, and the angular part $\Omega_i \equiv \{\theta_i, \hat{\mathbf{x}}_i, \hat{\mathbf{y}}_i\}$ denotes a set of hyperspherical angles, with hyperangle $\theta_i = \arctan(x_i/y_i)$, and others angles associated with the unit vectors $\hat{\mathbf{x}}_i$ and $\hat{\mathbf{y}}_i$. The projection of Faddeev components ψ_Y and ψ_α, hereafter shown as ψ_Q, for a given total angular momentum j and its projection μ onto the spherical coordinates is given by [72, 73],

$$\psi_Q^{j\mu}(\rho_i, \Omega_i) = \rho_i^{-5/2} \sum_\beta \mathcal{R}_\beta^j(\rho_i)\mathcal{Y}_\beta^{j\mu}(\Omega_i), \quad (4)$$

$\mathcal{Y}_\beta^{j\mu}(\Omega_i)$ is written in terms of hyperspherical harmonics $\Upsilon_{Kl}^{l_{x_i} l_{y_i}}(\Omega_i)$, which is eigenstates of the hypermomentum harmonics operator $\hat{K}$ as

$$\mathcal{Y}_\beta^{j\mu}(\Omega) = \left\{ \left[\Upsilon_{Kl}^{l_x l_y}(\Omega) \otimes \phi_{S_x} \right]_{j_{ab}} \otimes \kappa_I \right\}_{j\mu}, \quad (5)$$

$$\Upsilon_{Klm_l}^{l_x l_y}(\Omega) = \varphi_K^{l_x l_y}(\theta) \left[Y_{l_x}(\hat{x}) \otimes Y_{l_y}(\hat{y}) \right]_{lm_l}, \quad (6)$$

$$\varphi_K^{l_x l_y}(\theta) = N_K^{l_x l_y} (\sin\theta)^{l_x} (\cos\theta)^{l_y} P_n^{l_x+1/2, l_y+1/2}(\cos 2\theta), \quad (7)$$

where $P_n^{a,b}$ is the Jacobi polynomial by order $n = (K - l_x - l_y)/2$ and $N_K^{l_x l_y}$ is a normalizing coefficient. The $\beta \equiv \{K, l_x, l_y, l, S_x, j_{ab}\}$ represents a set of quantum numbers of a specific channel coupled to j. K is the hyperangular quantum number, l_x and l_y are the orbital angular momenta of the Jacobi coordinates x and y, $\mathbf{l} = \mathbf{l_x} + \mathbf{l_y}$ is total orbital angular momentum, S_x is the total spin of the pair particles associated with the coordinate x, and $\mathbf{j_{ab}} = \mathbf{l} + \mathbf{S_x}$. $\mathbf{I}$ denotes the spin of the third particle and the total angular momentum j is $\mathbf{j} = \mathbf{j_{ab}} + \mathbf{I}$. In Eq. (5), ϕ_{S_x} is the spin wave function of two-body subsystem, and κ_I is the spin function of the third particle. Applying this expansion in the Faddeev equations, and performing the hyperangular integration, one obtains a set of coupled differential equations for the wave functions $\mathcal{R}_\beta^j(\rho)$ of Eq. (4) as

$$\left[-\frac{\hbar^2}{2m}\left(\frac{d^2}{d\rho^2} - \frac{(K+3/2)(K+5/2)}{\rho^2} \right) - E \right] \mathcal{R}_\beta^j(\rho) + \sum_{\beta'} V_{\beta\beta'}^{j\mu}(\rho)\mathcal{R}_{\beta'}^j(\rho) = 0, \quad (8)$$

The coupling potentials are the hyperangular integrations of the two-body interaction $V_{\beta\beta'}^{j\mu}(\rho_i) = \left\langle \mathcal{Y}_\beta^{j\mu}(\Omega_i) \middle| \hat{V}_{ij} \middle| \mathcal{Y}_{\beta'}^{j\mu}(\Omega_j) \right\rangle$ and the $\hat{V}_{ij}$ are the two-body potentials between particles i and j, which will be introduced in Section 3.

In order to solve these coupled equations the hyperradial wave functions $\mathcal{R}_\beta^j(\rho)$ are expanded in a finite basis set of i_{max} hyperradial excitations as

$$\mathcal{R}_\beta^j(\rho) = \sum_{i=0}^{i_{max}} C_{i\beta}^j R_{i\beta}(\rho), \quad (9)$$

where the coefficients $C_{i\beta}^j$ can be obtained by diagonalizing the three-body Hamiltonian for $i = 0, ..., i_{max}$ basis

functions. The hyperradial functions $R_{i\beta}(\rho)$ can be written in terms of Laguerre polynomials.

By having three-body wave function $\Psi^{j\mu}$ in the hyperspherical coordinates, one can study the geometrical structure of $YY\alpha$ systems by calculating the matter radius $r_{mat}=\sqrt{\langle r^2\rangle}$, and the correlation densities, the probability to have definite distances between the particles in the three-body system

$$P(r_{jk},r_{(jk)i})=\frac{r_{jk}^2 r_{(jk)i}^2}{2j+1}\sum_{\mu}\int d\hat{x}_i d\hat{y}_i\left|\psi^{j\mu}(x_i,y_i)\right|^2. \quad (10)$$

3 Two-body potentials

In this section, we present the two-body interactions that we use in our calculations for the bound state of $\Lambda\Lambda\alpha$ and $\Omega\Omega\alpha$ three-body systems.

3.1 $\Lambda\Lambda\alpha$ System

For $\Lambda\Lambda$ interaction, we use HAL QCD potentials in $^1S_0$ channel with isospin $T=0$ [4]

$$V_{\Lambda\Lambda}(r)=\sum_{i=1}^{2}\alpha_i\exp(-r^2/\beta_i^2) \quad (11)$$

$$+\lambda_2\left(1-\exp(-r^2/\rho_2^2)\right)^2\left(\frac{\exp(-m_\pi r)}{r}\right)^2.$$

The effective $\Lambda\Lambda$ interaction is handled by the coupled-channel formalism [74] at three imaginary-time distances of $t/a=11,12,13$, where the potential parameters are fitted to $\chi^2/d.o.f=1.30(40)$, $0.76(18)$, and $0.74(30)$, respectively. The t-dependence is insignificant within the statistical errors. The fitted potential parameters to Eq. (11) are given in Table 1, where the pion mass is $m_\pi=146$ MeV.

The low-energy data derived with this interaction indicate no bound or resonant di-hyperon exists around the $\Lambda\Lambda$ threshold in (2+1)-flavor QCD at nearly physical quark masses, and predict a scattering length $a_0^{(\Lambda\Lambda)}=-0.81\pm0.23^{+0.00}_{-0.13}$ fm and an effective range $r_{\rm eff}^{(\Lambda\Lambda)}=5.47\pm0.78^{+0.09}_{-0.55}$ fm. The central values and the statistical errors are extracted from phase shifts at $t/a=12$, and the systematic errors are estimated from the central values at $t/a=11$ and 13[4]. The systematic errors are estimated by the difference between the results obtained by the fit range, and the statistical errors are estimated by the jackknife sampling of the lattice QCD configurations. The source of systematic error is the contamination from inelastic states.

Table 1: The fitted parameters of $V_{\Lambda\Lambda}(r)$ potential, shown in Eq. (11), taken from Ref. [4]. The statistical errors in fitted parameters are not taken into account in our calculations.

t/a	α_1 (MeV)	β_1 (fm)	α_2 (MeV)	β_2 (fm)	λ_2 (MeV $\cdot$ fm^2)	ρ_2 (fm)
11	1466.4	0.160	407.1	0.366	−170.3	0.918
12	1486.7	0.156	418.2	0.367	−160.0	0.929
13	1338.0	0.143	560.7	0.322	−176.2	1.033

For the $\Lambda\alpha$ interaction we use the Isle-type Gaussian potential [14]

$$V_{\Lambda\alpha}(r)=450.4\exp(-(r/1.25)^2)-404.9\exp(-(r/1.41)^2). \quad (12)$$

This potential reproduces the experimental data for the lifetime and binding energy of the ${}^{5}_{\Lambda}He$ hypernucleus with $\tau=3.02^{+0.10}_{-0.09}\times10^{-10}$ s and $E_B=-3.1$ MeV [75].

3.2 $\Omega\Omega\alpha$ System

The HAL QCD $\Omega\Omega$ potential in $^1S_0$ channel is fitted to an analytical function as [2]

$$V_{\Omega\Omega}(r)=\sum_{j=1}^{3}c_j e^{-(r/d_j)^2}, \quad (13)$$

where the potential parameters, without considering the statistical errors, are $(c_1,\ c_2,\ c_3)=(914,\ 305,\ -112)$ MeV and $(d_1,\ d_2,\ d_3)=(0.143,\ 0.305,\ 0.949)$ fm. Using a single-folding potential method, an $\Omega\alpha$ interaction has been recently extracted from a separable HAL QCD ΩN potential. This potential supports an $\Omega\alpha$ bound state with the binding energy of about -22 MeV and is parameterized in the form of the Woods-Saxon type potential [76]

$$V_{\Omega\alpha}(r)=-61\left(1+\exp\left(\frac{r-1.7}{0.47}\right)\right)^{-1}. \quad (14)$$

All two-body interactions for YY ($\Lambda\Lambda$ and $\Omega\Omega$) and also $Y\alpha$ ($\Lambda\alpha$ and $\Omega\alpha$) subsystems are shown in Fig. 2.

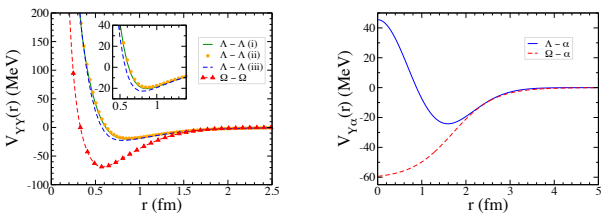

Fig. 2: Left panel: the YY potentials for three models of HAL QCD $\Lambda\Lambda$ potential of Eq. (11) with the parameters given in Table 1 at the imaginary-time distances $t/a = 11, 12, 13$ (shown as model i, ii, iii); and the HAL QCD $\Omega\Omega$ potential of Eq. (13). Right panel: the $Y\alpha$ potentials for the Isle-type $\Lambda\alpha$ potential given in Eq. (12); and the Woods-Saxon type $\Omega\alpha$ potential given in Eq. (14).

In our calculations we consider the Coulomb interaction in the $\Omega\Omega\alpha$ system using a hard-sphere model as [77]

$$V_{Coul}(r) = Z^2 e^2 \times \begin{cases} \frac{1}{r_{Coul}} \left(\frac{3}{2} - \frac{r^2}{2r_{Coul}^2} \right), & r \le r_{Coul} \\ \frac{1}{r}, & r > r_{Coul} \end{cases} \quad (15)$$

with a Coulomb radius $r_{Coul} = 1.47$ fm.

4 Results and discussion

To calculate the ground state binding energy and the geometrical properties of $\Lambda\Lambda\alpha$ and $\Omega\Omega\alpha$, we solve the coupled Faddeev equations (2) by implementing the FaCE computational toolkit [78] using the two-body interactions discussed in Sec. 3. To discretize the continuous hyperradius coordinate ρ_i, we use the Gauss–Laguerre quadrature with 100 grid points, and the hyperangular integrations are performed using Gauss-Jacobi quadrature with 60 grid points. The hyperradius cutoffs are selected high enough to achieve the cutoff-independent binding energies, converging with four significant figures. In our calculations, the mass of particles are m_N=939 MeV, m_Λ=1127.42 MeV, m_Ω = 1672.45, and m_α=3727.38 MeV. Table 2 shows the convergence of three-body ground state binding energy E_3 and nuclear matter radius r_{mat} as a function of maximum values of hyperangular quantum number K_{max} and hyperradial excitations i_{max}. The spin and isospin of $\Lambda\Lambda\alpha$ and $\Omega\Omega\alpha$ systems are equal to zero. The number of strange quark content for $\Lambda\Lambda\alpha$ and $\Omega\Omega\alpha$ is equal to 2 and 6, respectively. The Coulomb interaction of Eq. (15) is considered in $\Omega\Omega\alpha$ systems leading to an increase of about 6 MeV in 3B binding energy.

Since $\Omega\alpha$ interaction is completely attractive, faster convergence is reached in the calculation of ground state binding energy and nuclear matter radius of $\Omega\Omega\alpha$ to -67.21 MeV and 1.326 fm. For $\Lambda\Lambda\alpha$ system a convergence can be reached at larger values of K_{max} and i_{max}. For $\Lambda\Lambda\alpha$, the ground state binding energy and nuclear matter radius converge to -7.468 MeV and 1.955 fm. The listed results for $\Lambda\Lambda\alpha$ are obtained for $\Lambda\Lambda$ interaction with imaginary-time distance $t/a = 12$, whereas for $t/a = 11$ and $t/a = 13$, the calculated ground state binding energies are -7.605 MeV and -7.804 MeV, correspondingly.

Table 2: The convergence of three-body ground state binding energy E_3 and nuclear matter radius r_{mat} calculated for $\Lambda\Lambda\alpha$ and $\Omega\Omega\alpha$ systems as a function of maximum hyperradial excitations i_{max} (with $K_{max} = 80$) and hyperangular quantum number K_{max} (with $i_{max} = 25$).

	$\Lambda\Lambda\alpha$		$\Omega\Omega\alpha$	
i_{max}	E_3 (MeV)	r_{mat} (fm)	E_3 (MeV)	r_{mat} (fm)
5	−7.442	1.930	−67.19	1.327
10	−7.467	1.954	−67.21	1.326
15	−7.468	1.955	−67.21	1.326
20	−7.468	1.955	−67.21	1.326
25	−7.468	1.955	−67.21	1.326
K_{max}	E_3 (MeV)	r_{mat} (fm)	E_3 (MeV)	r_{mat} (fm)
5	−6.897	1.953	−66.58	1.327
10	−7.321	1.948	−67.04	1.326
15	−7.404	1.951	−67.14	1.326
20	−7.446	1.953	−67.19	1.326
25	−7.456	1.954	−67.20	1.326
30	−7.463	1.955	−67.21	1.326
35	−7.465	1.955	−67.21	1.326
40	−7.466	1.955	−67.21	1.326
45	−7.467	1.955	−67.21	1.326
50	−7.467	1.955	−67.21	1.326
55	−7.467	1.955	−67.21	1.326
60	−7.468	1.955	−67.21	1.326
65	−7.468	1.955	−67.21	1.326
70	−7.468	1.955	−67.21	1.326
75	−7.468	1.955	−67.21	1.326
80	−7.468	1.955	−67.21	1.326

In Table 3, beside the converged 3B binding energies for $\Lambda\Lambda\alpha$ and $\Omega\Omega\alpha$ systems, we list the binding energy of two-body YY and $Y\alpha$ subsystems. Furthermore, the 3B binding energies in which the 2B interactions between identical hyperons are set to zero, *i.e.*, $V_{YY}=0$, are also listed. Our numerical results show that the relative percentage difference $(B_3(V_{YY}=0)-2B_2(V_{Y\alpha}))/B_3(V_{YY}=0)\times 100$ varies between 4 to 6%. As one can see in Table 3, the $\Omega\Omega\alpha$ has a deeper bound state by having two bound subsystems. Our numerical analysis shows that the uncertainties in the HAL QCD $\Omega\Omega$ ($\Lambda\Lambda$) potential parameters impact the ${}^{6}_{\Omega\Omega}$He (${}^{6}_{\Lambda\Lambda}$He) ground state binding energy for about 4 (0.1) MeV and the r_{mat} for less than 0.01 (0.007) fm. While the employed $\Omega\alpha$ potential in our calculations is derived based on the dominant ${}^5S_2$ channel of $N\Omega$ interactions [3, 79], the contribution of the ${}^3S_1$ channel can be reasonably ignored. While the implemented two-body interactions in our calculations are restricted to only one angular momentum channel, we should point out that to the best of our knowledge, no lattice two-body interactions developed to higher channels. This restriction in the interactions should explain the deep binding of the Ω particles to the α as possible contributions of repulsive channels are not taken into account, even though their contributions appear to be small [79].

In Table 4 we compare our numerical results with other theoretical results such as gaussian expansion method (GEM), stochastic variational method (SVM), differential Faddeev equations (DFE), quark-cluster-model (QCM) by different YY interaction models like Nijmegen model D (ND), simulating Nijmegen hard-core model F (NF_s), modified simulating Nijmegen hard-core model D (mND_s), simulating Nijmegen hard-core model D (ND_s), spin-flavor $SU6$ quark-model (fss2), Nijmegen soft-core model (NSC97e), G-matrix interaction based on the bare ND interaction (ND(G)), Nijmegen extended soft-Core (ESC00) and finally experimental data (Exp).

Table 3: Three-body ground state binding energies E_3 in MeV for $YY\alpha$ systems. The last column shows our results for 3B binding energies with zero interaction in YY subsystems. Two-body binding energies E_2 for YY and $Y\alpha$ subsystems are also shown in MeV.

$YY\alpha$ System	E_2 (YY)	E_2 $(Y\alpha)$	E_3	E_3 $(V_{YY}=0)$
$\Lambda\Lambda\alpha$ $(t/a=12)$	Not Bound	-3.146	-7.468	-6.463
$\Omega\Omega\alpha$	-1.408	-22.01	-67.21	-48.96

Table 4: A comparison between our results for three-body ground state binding energy E_3 of $\Lambda\Lambda\alpha$ system and other theoretical and experimental data.

Ref.	YY Model	E_3 (MeV)
present	HAL QCD $(t/a=11)$	-7.605
present	HAL QCD $(t/a=12)$	-7.468
present	HAL QCD $(t/a=13)$	-7.804
[10] (GEM)	ND	-7.25
[12] (SVM)	NF_s	-7.52
[12] (SVM)	mND_s	-7.53
[12] (SVM)	ND_s	-7.93
[80] (DFE)	fss2	-7.653
[14] (DFE)	NSC97e	-6.82
[14] (DFE)	ND	-9.10
[14] (DFE)	ND(G)	-10.1
[14] (DFE)	ESC00	-10.7
[81] (QCM)	ND	-9.7
[81] (QCM)	ND(G)	-9.4
[82] (GEM)	ND	-9.34
[83] (G-matrix)	ND(G)	-9.23
[47, 48] (Exp.)	–	-6.91 ± 0.16
[45] (Exp.)	–	-7.25 ± 0.19
[49] (Exp.)	–	-10.9 ± 0.8

By having 3B wave functions of $YY\alpha$ systems in terms of the HH basis, we calculate the geometrical quantities, *i.e.*, the r.m.s. distances between the particles and the r.m.s. matter radius, presented in Table 5. In our calculations, we consider the α matter radius of 1.47 fm. For comparison, we also present the DFE results of Ref. [14]. Since the studied 3B systems consist of two identical hyperons and one alpha particle, interacting by scalar potentials, three particles form a ground state where the most probable positions of the particles have the shape of an isosceles triangle. As it is shown in Table 5, our numerical results for the expectation values of the Jacobi coordinates in (YY,α) and $(Y\alpha,Y)$ configurations satisfy the following Pythagorean theorem with high accuracy

$$\Delta=\langle r_{(YY)\alpha}\rangle^2+\frac{1}{4}\langle r_{YY}\rangle^2-\langle r_{Y\alpha}\rangle^2=0. \qquad (16)$$

Table 5: The expectation values of Jacobi coordinates in $\Lambda\Lambda\alpha$ and $\Omega\Omega\alpha$ systems. $\langle r_{YY}\rangle$ is the separation between identical hyperons, $\langle r_{Y\alpha}\rangle$ is the separation between $Y\alpha$ pairs, $\langle r_{(YY)\alpha}\rangle$ is the separation between the center of mass of YY pair and the spectator α particle. $\langle\rho^2\rangle^{1/2}$ is r.m.s. matter radius of the three-body system containing only point particles, and r_{mat} is the r.m.s. matter radius. The numbers in parentheses are from the DFE calculations by using the Nijmegen model D (ND) YY interaction [14]. Δ shows the accuracy of satisfaction of the Pythagorean theorem in Eq. (16).

$(YY\alpha)$ System	$\langle r_{YY}\rangle$ (fm)	$\langle r_{Y\alpha}\rangle$ (fm)	$\langle r_{(YY)\alpha}\rangle$ (fm)	$\lvert\Delta\rvert$ (fm^2)	$\langle\rho^2\rangle^{1/2}$ (fm)	r_{mat} (fm)
$\Lambda\Lambda\alpha$ $(t/a=11)$	3.598 (3.36)	2.902 (2.70)	2.276 (2.11)	0.005 (0.015)	3.943	1.944
$\Lambda\Lambda\alpha$ $(t/a=12)$	3.629	2.926	2.295	0.002	3.976	1.955
$\Lambda\Lambda\alpha$ $(t/a=13)$	3.555	2.867	2.248	0.007	3.895	1.929
$\Omega\Omega\alpha$	1.521	1.293	1.047	0.003	2.037	1.326

Table 6: The contributions of different partial wave channels W to the total norm of 3B ground state wave functions of $\Lambda\Lambda\alpha$ and $\Omega\Omega\alpha$ systems. For each system, the upper panel shows the contributions in $(Y\alpha-Y)$ Jacobi coordinates, and the lower panel shows the contributions in $(YY-\alpha)$ Jacobi coordinates. Channels with a contribution greater than 0.001% are listed.

K	l_{x_i}	l_{y_i}	l	S_{x_i}	j_{ab}	W
			$(\Lambda\alpha-\Lambda)$ Jacobi			
0	0	0	0	0.0	0.0	0.980
2	0	0	0	0.0	0.0	0.004
4	2	2	0	0.0	0.0	0.012
			$(\Lambda\Lambda-\alpha)$ Jacobi			
0	0	0	0	0.5	0.5	0.980
2	1	1	0	0.5	0.5	0.004
4	1	1	0	0.5	0.5	0.001
4	0	0	0	0.5	0.5	0.010
			$(\Omega\alpha-\Omega)$ Jacobi			
0	0	0	0	0.0	0.0	0.993
2	0	0	0	0.0	0.0	0.005
			$(\Omega\Omega-\alpha)$ Jacobi			
0	0	0	0	1.5	1.5	0.993
2	1	1	0	1.5	1.5	0.005

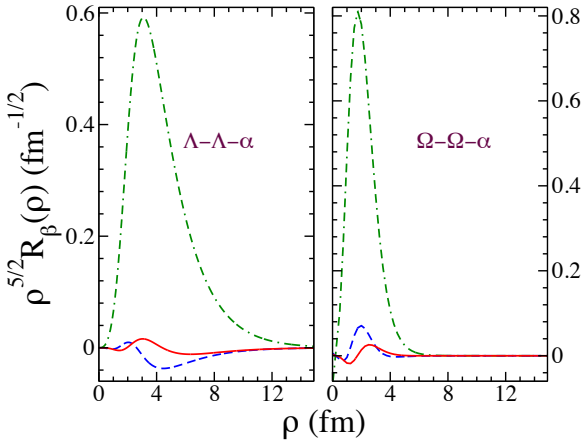

Fig. 3: The hyperradial wave function $\rho^{5/2}R_\beta(\rho)$ for the first three dominant channels, $\beta\equiv\{0,0,0,0,0,0\}$ (green dash-dotted line), $\beta\equiv\{2,0,0,0,0,0\}$ (blue dashed line), and $\beta\equiv\{4,0,0,0,0,0\}$ (red solid line), of the ground state wave functions of $\Lambda\Lambda\alpha$ and $\Omega\Omega\alpha$ systems.

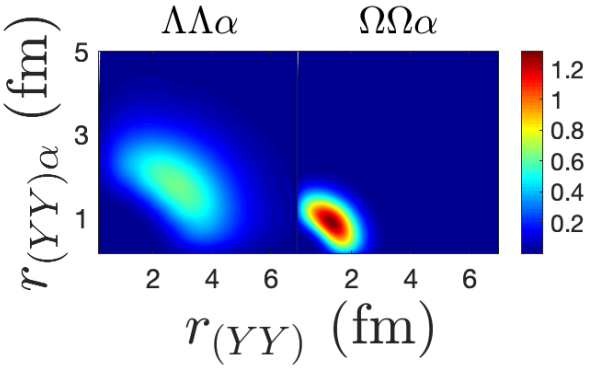

Fig. 4: The 3B ground state probability density of $\Lambda\Lambda\alpha$ and $\Omega\Omega\alpha$ systems as a function of $\langle r_{YY}\rangle$, the distance between YY pair, and $r_{(YY)\alpha}$, the distance between α particle and the center of mass of the YY pair.

In Table 6, we present the contribution of different channels, indicated by the quantum numbers $\{K,l_{x_i},l_{y_i},l,S_{x_i},j_{ab}\}$, to the total norm of 3B ground state wave functions of $\Lambda\Lambda\alpha$ and $\Omega\Omega\alpha$ systems in both $(Y\alpha-Y)$ and $(YY-\alpha)$ Jacobi coordinates. As one can see, the main contributions in 3B wave functions come from the $s-$wave channels, and the higher partial wave channels substantially have an insignificant contribution.

In Fig. 3, we show the first three dominant hyperradial components $\rho^{5/2}R_\beta(\rho)$ for the ground state wave functions of $\Lambda\Lambda\alpha$ and $\Omega\Omega\alpha$ systems, obtained by $i_{max}=25$. As the binding energy of the 3B system is increasing from the left to the right panel, the system is becoming more compact in the configuration space. In Fig. 4, we illustrate the probability density of 3B ground states of $\Lambda\Lambda\alpha$ and $\Omega\Omega\alpha$ systems as a function of $\langle r_{YY}\rangle$, the distance between the two identical Y hyperons, and $r_{(YY)\alpha}$, the distance between α particle and the center of mass of two Y particles. As we can see for both systems, the distributions along the $\langle r_{YY}\rangle$ direction are broader than the $r_{(YY)\alpha}$ direction,

confirming that the distance between identical Y hyperons is greater than the distance of the spectator α particle and the center of mass of the YY pair.

5 Summary and Outlook

In this paper, we study the ground-state properties of multi-strangeness hypernuclei ${}^{6}_{\Lambda\Lambda}$He and ${}^{6}_{\Omega\Omega}$He in a hyperharmonic three-body model of $(YY\alpha)$. To this aim, we solve two coupled Faddeev equations in configuration space with the hyperspherical harmonics expansion method using the most modern two-body interactions, including the recent lattice QCD potentials, to calculate the ground state binding energies and geometrical properties. In our numerical analysis, we check the convergence of 3B ground state binding energies and nuclear matter radii as a function of the maximum value of hyperradial excitations i_{max} and hyperangular quantum number K_{max}. Our numerical results show that the ground state binding energy of ${}^{6}_{\Lambda\Lambda}$He using three models of $\Lambda\Lambda$ lattice interactions changes in the domain $(-7.468,\ -7.804)$ MeV while ${}^{6}_{\Omega\Omega}$He has deep binding energy of -67.21 MeV. We should indicate that implemented $\Omega\alpha$ potential in our calculations is restricted to only one angular momentum channel, and the contribution of repulsive channels is not considered. So this could explain the deep binding of the $\Omega\alpha$ and consequently the ${}^{6}_{\Omega\Omega}$He system.

We study the geometrical properties of the aforemen-

tioned ^{6}He double hyperon by calculating the expectation values of the Jacobi coordinates and the r.m.s. matter radius and correlation density. Our numerical results confirm that the studied 3B systems, composed of two identical hyperons and one alpha particle, form isosceles triangles where the most probable positions of the particles perfectly satisfy the Pythagorean theorem. Our numerical analysis on the structure of 3B ground state wave functions shows that the main contributions of over 99% are from the $s-$wave channels. Our numerical results for ${}^{~6}_{\Lambda\Lambda}$He are in agreement with other theoretical studies.

Considering the contributions of the coupled channels in $\Lambda\Lambda-\Xi N$ ($\Omega N-\Lambda\Xi-\Sigma\Xi$) interactions is a complementary task to be implemented in the FaCE toolkit to include the coupled components in the wave function of ${}^{~6}_{\Lambda\Lambda}$He (${}^{~6}_{\Omega\Omega}$He). As it is shown in Refs. [81, 84], the contribution of the coupled channels leads to an increase of about $0.1\sim0.4$ MeV in the $\Lambda\Lambda\alpha$ binding energy while using an effective single-channel interaction leads to a reduction of about 0.3 MeV [14]. This reduction is due to the tight α cluster binding, which inhibits the effectiveness of the $\Lambda\Lambda-\Xi N$ coupling, and we assume that this should also be valid for the $\Omega\Omega\alpha$ system. Moreover, while the contribution of transition potentials to the inelastic channels [85], *i.e.*, $\Omega N-\Lambda\Xi-\Sigma\Xi$ are expected to be small [79], they have not yet been derived from the lattice QCD calculations and can be considered in a future study when they are developed.

Acknowledgement

F.E. thanks T. Hatsuda and J. Casal for helpful discussions and suggestions. The work of M.R.H. was supported by the National Science Foundation under Grant No. NSF-PHY-2000029 with Central State University.

References

1 N. K. Glendenning. Uncertainty of hyperon couplings and the electrochemical potential in neutron star matter. *Phys. Rev. C*, 64:025801, Jun 2001. URL https://doi.org/10.1103/PhysRevC.64.025801.

2 S. Gongyo et al. Most Strange Dibaryon from Lattice QCD. *Phys. Rev. Lett.*, 120:212001, May 2018. URL https://doi.org/10.1103/PhysRevLett.120.212001.

3 T. Iritani et al. NΩ dibaryon from lattice QCD near the physical point. *Phys. Lett. B*, 792:284–289, 2019. ISSN 0370-2693. URL https://doi.org/10.1016/j.physletb.2019.03.050.

4 K. Sasaki et al. $\Lambda\Lambda$ and NΞ interactions from lattice QCD near the physical point. *Nucl. Phys. A*, 998:121737, 2020. URL https://doi.org/10.1016/j.nuclphysa.2020.121737.

5 N. Ishii, S. Aoki, and T. Hatsuda. Nuclear Force from Lattice QCD. *Phys. Rev. Lett.*, 99:022001, Jul 2007. URL https://doi.org/10.1103/PhysRevLett.99.022001.

6 N. Ishii et al. Hadron–hadron interactions from imaginary-time Nambu$-$Bethe$-$Salpeter wave function on the lattice. *Phys. Lett. B*, 712(4):437–441, 2012. ISSN 0370-2693. URL https://doi.org/10.1016/j.physletb.2012.04.076.

7 Z. Y. Zhang et al. Suggesting a di-omega dibaryon search in heavy ion collision experiments. *Phys. Rev. C*, 61:065204, May 2000. doi: 10.1103/PhysRevC.61.065204. URL https://link.aps.org/doi/10.1103/PhysRevC.61.065204.

8 Hongxia Huang, Jialun Ping, and Fan Wang. Further study of the $N\Omega$ dibaryon within constituent quark models. *Phys. Rev. C*, 92:065202, Dec 2015. doi: 10.1103/PhysRevC.92.065202. URL https://link.aps.org/doi/10.1103/PhysRevC.92.065202.

9 E. Hiyama et al. Four-body cluster structure of $A=7-10$ double-Λ hypernuclei. *Phys. Rev. C*, 66:024007, Aug 2002. URL https://doi.org/10.1103/PhysRevC.66.024007.

10 E. Hiyama and K. Nakazawa. Structure of $S=-2$ Hypernuclei and Hyperon–Hyperon Interactions. *Annu. Rev. Nucl. Part. Sci.*, 68(1):131–159, 2018. URL https://doi.org/10.1146/annurev-nucl-101917-021108.

11 H. Nemura et al. Study of light Λ and $\Lambda\Lambda$ hypernuclei with the stochastic variational method and effective ΛN potentials. *Prog. Theor. Phys.*, 103:929–958, 2000. URL https://doi.org/10.1143/PTP.103.929.

12 H. Nemura et al. Fully Coupled Channel Approach to Doubly Strange s-Shell Hypernuclei. *Phys. Rev. Lett.*, 94:202502, May 2005. URL https://doi.org/10.1103/PhysRevLett.94.202502.

13 I. N. Filikhin and A. Gal. Light $\Lambda\Lambda$ hypernuclei and the onset of stability for $\Lambda\Xi$ hypernuclei. *Phys. Rev. C*, 65:041001, Apr 2002. URL https://doi.org/10.1103/PhysRevC.65.041001.

14 I. N. Filikhin and A. Gal. Faddeev$-$Yakubovsky calculations for light $\Lambda\Lambda$ hypernuclei. *Nucl. Phys. A*, 707(3):491–509, 2002. ISSN 0375-9474. URL https://doi.org/10.1016/S0375-9474(02)01008-4.

15 I. N. Filikhin, V. M. Suslov, and B Vlahovic. Bound state of the $\alpha\Lambda\Lambda\Xi^0$ system. *J. Phys. G: Nucl. Part. Phys.*, 35(3):035103, 2008. URL https://doi.org/10.1088/0954-3899/35/3/035103.

16 I. N. Filikhin, V. M. Suslov, and B. Vlahovic. Faddeev calculations for light Ξ-hypernuclei. *Math. Model. Geom.*, 5(2):1–11, 2017. URL http://mmg.tversu.ru/images/publications/2017-vol5-n2/Filikhin-2017-04-19.pdf.

17 L. Contessi et al. The onset of $\Lambda\Lambda$ hypernuclear binding. *Phys. Lett. B*, 797:134893, 2019. ISSN 0370-2693. URL https://doi.org/10.1016/j.physletb.2019.134893.

18 Hoai Le et al. S-shell $\Lambda\Lambda$ hypernuclei based on chiral interactions. *Eur. Phys. J. A*, 57:217, 2021. URL https://doi.org/10.1140/epja/s10050-021-00522-8.

19 L. Fabbietti, V. Mantovani Sarti, and O. Vázquez Doce. Study of the Strong Interaction Among Hadrons with Correlations at the LHC. *Annu. Rev. Nucl. Part. Sci.*, 71(1):377–402, 2021. URL https://doi.org/10.1146/annurev-nucl-102419-034438.

20 S. Acharya et al. Unveiling the strong interaction among hadrons at the LHC. *Nature*, 588(7837):232, 2020. URL https://doi.org/10.1038/s41586-020-3001-6.

21 J. Adam et al. Measurement of the mass difference and the binding energy of the hypertriton and antihypertriton. *Nat. Phys.*, 16:409, 2020. ISSN 1745-2481. URL https://doi.org/10.1038/s41567-020-0799-7.

22 H. Le et al. Implications of an increased Λ-separation energy of the hypertriton. *Phys. Lett. B*, 801:135189, 2020. ISSN 0370-2693. URL https://doi.org/10.1016/j.physletb.2019.135189.

23 H. Garcilazo, A. Valcarce, and T. F. Caramés. The N$\Lambda\Lambda-\Xi$NN bound state problem. *J. Phys. G: Nucl. Part. Phys.*, 41(9):095103, jul 2014. URL https://doi.org/10.1088/0954-3899/41/9/095103.

24 H. Garcilazo, A. Valcarce, and J. Vijande. Maximal isospin few-body systems of nucleons and Ξ hyperons. *Phys. Rev. C*, 94:024002, Aug 2016. URL https://doi.org/10.1103/PhysRevC.94.024002.

25 E. Hiyama et al. Possible Lightest Ξ Hypernucleus with Mod-

ern ΞN Interactions. *Phys. Rev. Lett.*, 124:092501, Mar 2020. URL https://doi.org/10.1103/PhysRevLett.124.092501.
26 M. M. Nagels, Th. A. Rijken, and Y. Yamamoto. Extended-soft-core Baryon-Baryon ESC08 model $III.S = -2$ Hyperon-hyperon/nucleon Interaction. *arXiv preprint arXiv:1504.02634*, 2015.
27 Th. A. Rijken and H-J. Schulze. Hyperon-hyperon interactions with the Nijmegen ESC08 model. *Eur. Phys. J. A*, 52(2):1–10, 2016. URL https://doi.org/10.1140/epja/i2016-16021-6.
28 F. Etminan et al. Spin-2 NΩ dibaryon from lattice QCD. *Nucl. Phys. A*, 928:89–98, 2014. ISSN 0375-9474. URL https://doi.org/10.1016/j.nuclphysa.2014.05.014. Special Issue Dedicated to the Memory of Gerald E Brown (1926-2013).
29 Steven E. Koonin. Proton pictures of high-energy nuclear collisions. *Phys. Lett. B*, 70(1):43–47, 1977. ISSN 0370-2693. URL https://www.sciencedirect.com/science/article/pii/0370269377903409.
30 W. Bauer, C. Gelbke, and S. Pratt. Hadronic Interferometry in Heavy-Ion Collisions. *Ann. Rev. Nuc. Part. Sci.*, 42(1): 77–98, 1992. URL https://doi.org/10.1146/annurev.ns.42.120192.000453.
31 L. Adamczyk et al. ΛΛ correlation function in Au+Au collisions at $\sqrt{s_{NN}} = 200$ GeV. *Phys. Rev. Lett.*, 114:022301, Jan 2015. URL https://link.aps.org/doi/10.1103/PhysRevLett.114.022301.
32 S. Acharya et al. $p-p, p-\Lambda$, and $\Lambda-\Lambda$ correlations studied via femtoscopy in pp reactions at $\sqrt{s} = 7$ TeV. *Phys. Rev. C*, 99: 024001, Feb 2019. URL https://link.aps.org/doi/10.1103/PhysRevC.99.024001.
33 K. Morita et al. Probing multistrange dibaryons with proton-omega correlations in high-energy heavy ion collisions. *Phys. Rev. C*, 94:031901, Sep 2016. URL https://link.aps.org/doi/10.1103/PhysRevC.94.031901.
34 J. Adam et al. The proton-Ω correlation function in Au + Au collisions at sNN = 200 GeV. *Phys. Lett. B*, 790:490–497, 2019. ISSN 0370-2693. URL https://doi.org/10.1016/j.physletb.2019.01.055.
35 C. B. Chitwood et al. Final-State Interactions between Noncompound Light Particles for ^{16}O-Induced Reactions on ^{197}Au at $\frac{E}{A} = 25$ MeV. *Phys. Rev. Lett.*, 54:302–305, Jan 1985. URL https://link.aps.org/doi/10.1103/PhysRevLett.54.302.
36 R. Kotte et al. On the space-time difference of proton and composite particle emission in central heavy-ion reactions at 400 A· MeV.
37 K. Wosińska et al. Correlations of neutral and charged particles in 40 Ar-58 Ni reaction at 77 MeV/u. *Eur. Phys. J. A*, 32 (1):55–59, 2007. URL https://link.springer.com/article/10.1140/epja/i2006-10279-1.
38 W. Rzesa et al. Femtoscopy of kaon-proton and kaon-deuteron from ALICE. *https://twiki.cern.ch/twiki/pub/Main/ WutStudents/raportWR.pdf*, 2019. URL https://indico.cern.ch/event/819610/contributions/3425246/attachments/1845730/3028148/hirg1605.pdf.
39 St. Mrówczyński and P. Słoń. Hadron-deuteron correlations and production of light nuclei in relativistic heavy-ion collisions. *Acta Phys. Pol. B*, 51(8):1739–1755, 2020. URL https://www.actaphys.uj.edu.pl/fulltext?series=Reg&vol=51&page=1739.
40 K. Wisniewksi. *presentation at "Meson2012", Kraków, Poland, 31 May - 5 June 2012,*. URL http://meson.if.uj.edu.pl/meson2012/talks/Wisniewski.pdf.
41 J. Haidenbauer. Exploring the Λ-deuteron interaction via correlations in heavy-ion collisions. *Phys. Rev. C*, 102:034001, Sep 2020. URL https://doi.org/10.1103/PhysRevC.102.034001.
42 K. Morita et al. Probing ΩΩ and $p\Omega$ dibaryons with femtoscopic correlations in relativistic heavy-ion collisions. *Phys. Rev. C*, 101:015201, Jan 2020. URL https://link.aps.org/doi/10.1103/PhysRevC.101.015201.
43 Liang Zhang, Song Zhang, and Yu-Gang Ma. Production of ΩNN and $\Omega\Omega N$ in ultra-relativistic heavy-ion collisions. *Eur. Phys. J. C*, 82(5):1–10, 2022.
44 G. Verde et al. $d-\alpha$ correlation functions and collective motion in Xe + Au collisions at E/A = 50 MeV. *Phys. Lett. B*, 653 (1):12–17, 2007. ISSN 0370-2693. URL https://doi.org/10.1016/j.physletb.2007.07.031.
45 H. Takahashi et al. Observation of a ${}^{6}_{\Lambda\Lambda}$He double hypernucleus. *Phys. Rev. Lett.*, 87:212502, Nov 2001. URL https://doi.org/10.1103/PhysRevLett.87.212502.
46 C. Amsler et al. Review of Particle Physics. *Phys. Lett. B*, 667(1):1–6, 2008. ISSN 0370-2693. URL https://doi.org/10.1016/j.physletb.2008.07.018.
47 K. Nakazawa. Double-Λ Hypernuclei via the Ξ$^-$ Hyperon Capture at Rest Reaction in a Hybrid Emulsion. *Nucl. Phys. A*, 835(1):207–214, 2010. ISSN 0375-9474. URL https://doi.org/10.1016/j.nuclphysa.2010.01.195. Proc. 10th Int. Conf. on Hypernuclear and Strange Particle Physics.
48 J. K. Ahn et al. Double-Λ hypernuclei observed in a hybrid emulsion experiment. *Phys. Rev. C*, 88:014003, Jul 2013. URL https://doi.org/10.1103/PhysRevC.88.014003.
49 D. J. Prowse. ${}^{6}_{\Lambda\Lambda}$He double hyperfragment. *Phys. Rev. Lett.*, 17:782–785, Oct 1966. URL https://doi.org/10.1103/PhysRevLett.17.782.
50 H. Ekawa et al. Observation of a Be double-Lambda hypernucleus in the J-PARC E07 experiment. *Prog. Theor. Exp. Phys.*, 2019(2), 02 2019. ISSN 2050-3911. URL https://doi.org/10.1093/ptep/pty149. 021D02.
51 H. Tamura. Strangeness nuclear physics. In *Proc. 8th Int. Conf. on Quarks and Nuclear Physics (QNP2018)*, page 011003, 2019. URL https://journals.jps.jp/doi/abs/10.7566/JPSCP.26.011003.
52 J. Yoshida et al. Status of J-PARC E07: Systematic study of double strangeness nuclei with hybrid emulsion method. In *AIP Conf. Proc*, volume 2130, page 020016. AIP Publishing LLC, 2019. URL https://aip.scitation.org/doi/abs/10.1063/1.5118384.
53 T. Motoba et al. Chapter III. Production, Structure an Decay of Light p-Shell Λ-Hypernuclei. *Prog. Theor. Phys. Suppl.*, 81: 42–103, 01 1985. ISSN 0375-9687. URL https://doi.org/10.1143/PTPS.81.42.
54 E. Hiyama and T. Yamada. Structure of light hypernuclei. *Prog. Part. Nucl. Phys*, 63(2):339–395, 2009. ISSN 0146-6410. URL https://doi.org/10.1016/j.ppnp.2009.05.001.
55 J. J. Griffin and J. A. Wheeler. Collective Motions in Nuclei by the Method of Generator Coordinates. *Phys. Rev.*, 108:311–327, Oct 1957. URL https://doi.org/10.1103/PhysRev.108.311.
56 S. Saito. Interaction between Clusters and Pauli Principle). *Prog. Theor. Phys.*, 41(3):705–722, 03 1969. ISSN 0033-068X. URL https://doi.org/10.1143/PTP.41.705.
57 E. Hiyama, Y. Kino, and M. Kamimura. Gaussian expansion method for few-body systems. *Prog. Part. Nucl. Phys*, 51(1): 223–307, 2003. ISSN 0146-6410. URL https://doi.org/10.1016/S0146-6410(03)90015-9.
58 E. Hiyama. Gaussian expansion method for few-body systems and its applications to atomic and nuclear physics. *Prog. Theor. Exp. Phys.*, 2012(1), 09 2012. ISSN 2050-3911. URL https://doi.org/10.1093/ptep/pts015. 01A204.
59 A. Tohsaki et al. Alpha Cluster Condensation in ^{12}C and ^{16}O. *Phys. Rev. Lett.*, 87:192501, Oct 2001. URL https://doi.org/10.1103/PhysRevLett.87.192501.
60 S. Bayegan, M. R. Hadizadeh, and M. Harzchi. Three-nucleon bound state in a spin-isospin dependent three dimensional approach. *Phys. Rev. C*, 77:064005, Jun 2008. URL https://link.aps.org/doi/10.1103/PhysRevC.77.064005.
61 M. R. Hadizadeh et al. Scaling Properties of Universal Tetramers. *Phys. Rev. Lett.*, 107:135304, Sep 2011.

URL https://link.aps.org/doi/10.1103/PhysRevLett.107.135304.

62 M. R. Hadizadeh, Lauro Tomio, and S. Bayegan. Solutions of the bound-state Faddeev-Yakubovsky equations in three dimensions by using NN and $3N$ potential models. *Phys. Rev. C*, 83:054004, May 2011. URL https://doi.org/10.1103/PhysRevC.83.054004.

63 M. R. Hadizadeh et al. Binding and structure of tetramers in the scaling limit. *Phys. Rev. A*, 85:023610, Feb 2012. URL https://doi.org/10.1103/PhysRevA.85.023610.

64 M. R. Hadizadeh, Ch. Elster, and W. N. Polyzou. Relativistic three-body bound state in a 3D formulation. *Phys. Rev. C*, 90:054002, Nov 2014. URL https://doi.org/10.1103/PhysRevC.90.054002.

65 M. R. Hadizadeh, M. Radin, and K. Mohseni. A three-dimensional momentum-space calculation of three-body bound state in a relativistic Faddeev scheme. *Sci. Rep.*, 10(1):1–11, 2020. URL https://doi.org/10.1038/s41598-020-58577-4.

66 D. R. Lehman and W. C. Parke. Shell structure of the A = 6 ground states from three-body dynamics. *Phys. Rev. C*, 28:364–382, Jul 1983. URL https://doi.org/10.1103/PhysRevC.28.364.

67 M. V. Zhukov et al. Bound state properties of Borromean halo nuclei: ^{12}He and ^{11}Li . *Phys. Rep.*, 231(4):151–199, 1993. ISSN 0370-1573. URL https://doi.org/10.1016/0370-1573(93)90141-Y.

68 D. V. Fedorov, A. S. Jensen, and K. Riisager. Three-body halos. II. From two- to three-body asymptotics. *Phys. Rev. C*, 50:2372–2383, Nov 1994. URL https://doi.org/10.1103/PhysRevC.50.2372.

69 S. Funada, H. Kameyama, and Y. Sakuragi. Halo structure and soft dipole mode of the ^{6}He nucleus in the α+ n+ n cluster model. *Nucl. Phys. A*, 575(1):93–117, 1994. URL https://doi.org/10.1016/0375-9474(94)90140-6.

70 V. I. Kukulin et al. Detailed study of the cluster structure of light nuclei in a three-body model (IV). Large space calculation for A = 6 nuclei with realistic nuclear forces. *Nucl. Phys. A*, 586(1):151–189, 1995. ISSN 0375-9474. URL https://doi.org/10.1016/0375-9474(94)00494-8.

71 I. J. Thompson and M. V. Zhukov. Effects of ^{10}Li virtual states on the structure of ^{11}Li. *Phys. Rev. C*, 49:1904–1907, Apr 1994. URL https://doi.org/10.1103/PhysRevC.49.1904.

72 J. Casal, M. Rodríguez-Gallardo, and J. M. Arias. Analytical transformed harmonic oscillator basis for three-body nuclei of astrophysical interest: Application to ^{6}He. *Phys. Rev. C*, 88:014327, Jul 2013. URL https://doi.org/10.1103/PhysRevC.88.014327.

73 J. Casal et al. Electric dipole response of low-lying excitations in the two-neutron halo nucleus ^{29}F. *Phys. Rev. C*, 102:064627, Dec 2020. URL https://doi.org/10.1103/PhysRevC.102.064627.

74 S. Aoki et al. Construction of energy-independent potentials above inelastic thresholds in quantum field theories. *Phys. Rev. D*, 87:034512, Feb 2013. URL https://doi.org/10.1103/PhysRevD.87.034512.

75 Y. Kurihara, Y. Akaishi, and H. Tanaka. Effect of ΛN repulsive core on pionic decay of ${}^{5}_{\Lambda}$He. *Phys. Rev. C*, 31:971–973, Mar 1985. URL https://doi.org/10.1103/PhysRevC.31.971.

76 F. Etminan and M. M. Firoozabadi. Simple Woods-Saxon-type form for $\Omega\alpha$ and $\Xi\alpha$ interactions using folding model. *Chin. Phys. C*, 44(5):054106, 2020. URL https://doi.org/10.1088/1674-1137/44/5/054106.

77 J. Casal. *Weakly-bound three-body nuclear systems: structure, reactions and astrophysical implications*. PhD thesis, Universidad de Sevilla, 2016. URL https://core.ac.uk/download/pdf/51404457.pdf.

78 I. J. Thompson, F. M. Nunes, and B. V. Danilin. FaCE: a tool for three body Faddeev calculations with core excitation. *Comput. Phys. Commun*, 161(1):87–107, 2004. ISSN 0010-4655. URL https://doi.org/10.1016/j.cpc.2004.03.007.

79 T. Sekihara, Y. Kamiya, and T. Hyodo. $N\Omega$ interaction: Meson exchanges, inelastic channels, and quasibound state. *Phys. Rev. C*, 98:015205, Jul 2018. URL https://link.aps.org/doi/10.1103/PhysRevC.98.015205.

80 Y. Fujiwara et al. Faddeev calculation of ${}^{6}_{\Lambda\Lambda}$He using SU_6 quark-model baryon-baryon interactions. *Phys. Rev. C*, 70:037001, Sep 2004. URL https://doi.org/10.1103/PhysRevC.70.037001.

81 T. Yamada and C. Nakamoto. Structure of light $S = -2$ nuclei and hyperon mixing. *Phys. Rev. C*, 62:034319, Aug 2000. URL https://doi.org/10.1103/PhysRevC.62.034319.

82 E. Hiyama et al. Three-and Four-Body Cluster Models of Hypernuclei Using the G-Matrix ΛN Interaction: ${}^{9}_{\Lambda}$Be, ${}^{13}_{\Lambda}$C, ${}^{6}_{\Lambda\Lambda}$He and ${}^{10}_{\Lambda\Lambda}$Be. *Prog. Theor. Phys.*, 97(6):881–899, 1997. URL https://doi.org/10.1143/PTP.97.881.

83 Y. Yamamoto et al. Hyperon-Nucleon and Hyperon-Hyperon Interactions in Nuclei. *Prog. Theor. Phys. Suppl.*, 117:361–389, 03 1994. ISSN 0375-9687. URL https://doi.org/10.1143/ptp.117.361.

84 S. B. Carr, I. R. Afnan, and B. F. Gibson. ${}^{6}_{\Lambda\Lambda}$He as a ΛΛ interaction constraint. *Nucl. Phys. A*, 625(1):143–166, 1997. ISSN 0375-9474. URL https://doi.org/10.1016/S0375-9474(97)00480-6.

85 H. Garcilazo and A. Valcarce. ΩNN and ΩΩN states. *Phys. Rev. C*, 99:014001, Jan 2019. URL https://doi.org/10.1103/PhysRevC.99.014001.